Int. J. Heat Mass Transfer. Vol. 36, No. 15, pp. 3703–3710, 1993
Printed in Great Britain

0017–9310/93 $6.00+0.00

Use of *in situ* conductivity measurements to calculate the flow field and heat transfer in continuous-flow electrophoresis

JÖRN HEINRICH,† MICHAEL J. CLIFTON‡§ and HORST WAGNER†

†Anorganische und Analytische Chemie und Radiochemie, Universität des Saarlandes, Im Stadtwald, W-6600 Saarbrücken 11, Germany; and ‡Laboratoire de Génie Chimique (CNRS U.R.A. 192), Université Paul Sabatier, 118, route de Narbonne, F-31062 Toulouse cedex, France

(*Received* 23 *September* 1992 *and in final form* 17 *March* 1993)

Abstract—Experimentally measured local conductivities have been used as input data to a numerical model describing three-dimensional fluid flow and heat transfer in continuous-flow electrophoresis. These calculations are used to show the effect of gravity on the flow field in a commercially available apparatus. Different membrane types and different carrier solutions have been studied. Experimental conditions likely to give rise to buoyancy-driven flow have been found.

1. INTRODUCTION

ELECTROPHORESIS is the migration of electrically charged particles or macromolecules in an electric field. It is well known as the basis of a range of very powerful analytical techniques applied to mixtures of biological molecules. However, these techniques only treat extremely small quantities of matter, so as methods for preparing usable amounts of a pure substance they are very fastidious. Continuous-flow electrophoresis (CFE) allows the same mixtures to be separated in a continuous manner and is thus well adapted to preparative applications. In this process, a buffer solution of known properties (pH, electrical conductivity, viscosity, etc.) flows in the laminar regime through a thin rectangular chamber. The sample containing the species to be separated is injected into this carrier buffer in the form of a fine filament of solution. Electrode compartments situated on either side of this chamber are used to apply an electric field across its width. The molecules of the sample are carried by convection down the length of the chamber while at the same time migrating laterally under the influence of the electric field. As each molecular species has a characteristic mobility, the different molecules present in the original filament will migrate at different rates in the lateral direction, thus dividing the one original filament into a number of filaments that can be collected separately at the chamber outlet. The lateral distance migrated by each protein is given by the product of its mobility with the field strength and its residence time in the electric field. For this process to work correctly, a perfectly stable flow pattern is essential. Any instability of the flow during the long collection phase will cause a serious loss of resolution.

Flow instabilities arise in this process because of buoyancy-driven convection due to non-uniformities in solution density. Of course, a certain difference in density between the sample filament and the surrounding carrier solution is hard to avoid, but there is another source of density variation that can be more serious: the non-uniformities in ion concentration and temperature that are found near the electrode compartments.

The electrode compartments are divided off from the separation chamber by ion-permeable membranes. These membranes allow the electric current to pass, while at the same time preventing gas bubbles or other products of electrode reactions from coming into the separation zone; by their low hydraulic permeability, they also ensure that the low-velocity carrier flow remains undisturbed by the rapid flow of the electrode solutions. But these membranes always carry fixed charges, so that the ratio of cation to anion flux through the membrane is different from that found in the solution, i.e. the membranes modify the transport numbers of the ions. In this way, there is an enrichment of the solution on one side of the membrane and a depletion on the other. This concentration polarization will directly cause density differences due to varying concentration. At the same time, the passage of the electric current through the conducting solution causes Joule heating of the carrier buffer and a cooling system is necessary for CFE to operate satisfactorily. The cooling temperature can be adjusted so as to minimize non-uniformities in temperature, but variations in ion concentration mean variations in solution conductivity and so variations in the rate of heat dissipation. Thus the concentration polarization near the membranes gives rise to temperature variations that in turn cause density variations, in addition to those directly due to concentration effects. In fact, both effects work in the

§Author to whom correspondence should be addressed.

NOMENCLATURE

A	Kohlrausch factor
c	molar concentration of solute
T	temperature
T_0	reference temperature, temperature of the cooling liquid
u, v, w	velocity components in the x-, y- and z-directions
u_0	reference velocity, mean axial velocity
x, y, z	coordinates.

Greek symbols

β	coefficient for the effect of solute concentration on density
κ	electrical conductivity
Λ^0	limiting molar conductivity at infinite dilution
ρ	density of the solution
ρ_w	density of water.

same direction: a zone of depleted solution is less dense than the bulk solution and it is also more resistive and so will be more strongly heated.

A three-dimensional numerical model representing the coupled flow field and heat transfer in CFE under steady-state conditions has already been presented in a previous paper [1]. In that work, the profiles of buffer concentration were largely hypothetical. Only the profile at the outlet was accessible to measurement and the profile was assumed to undergo no development in the flow direction. In the present work, similar calculations have been performed, but experimental measurements of the local solution conductivity within the chamber were used to represent the variations in buffer concentration. This allows a more realistic appraisal of the importance of membrane-induced disturbances in the CFE process.

2. MATERIALS AND METHODS

A commercially available CFE chamber was used, the VaP 21 FFE, manufactured by Bender & Hobein, Munich, Germany. This chamber was of overall length 330 mm, of width 100 mm and 1 mm in thickness. However, the part of the cell over which the field was applied was only 250 mm long, i.e. the length of the electrode compartments. The front wall of the chamber is uncooled, whereas the back wall is a water-cooled metal plate, covered by a 0.13 mm thick Teflon coating. The cooling liquid flows very rapidly, so there is no measurable change in temperature between the inlet and the outlet ($\Delta T < 0.1$ K). The maximum overall power dissipation in the experiments was 3.68 W. The carrier solution was made to flow downwards.

This commercial equipment was modified by incorporation of a specially developed potential-gradient and conductivity scanner [2, 3]. In the front wall, 4 rows of gold sensing-electrodes were implanted, with 61 electrodes in each row. These rows cross the chamber in the direction of the applied field; they are situated at 5, 10, 15 and 20 cm from the beginning of the field zone (see Fig. 1). Between each pair of neighbouring electrodes, conductivities and potential differences can be measured using a computer-controlled data acquisition system. Thus each row of electrodes gives a conductivity and a potential profile. This set-up also allows the dynamics of the process to be detected, i.e. the changes in local electrical properties of the chamber from the moment when the field is applied, but the latter possibility has not been explicitly used in the present work.

The electrolyte systems investigated as carrier solutions were sodium acetate, sodium nitrate, Tris/acetic acid and Tris/nitric acid, with concentrations ranging from 1×10^{-3} to 5×10^{-3} mol l^{-1}. The electrode solutions were of the same composition as the carrier electrolyte. To prevent any influence from the electrode reactions, the electrode solutions were discarded after their passage through the electrode compartment. The residence times were varied from 300 to 1200 s, corresponding to typical times for CFE. These

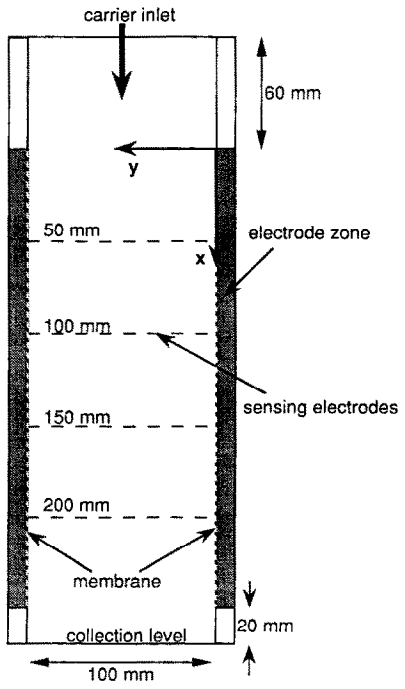

FIG. 1. Geometry of the experimental apparatus showing the positions of the rows of sensing electrodes used by the conductivity scanner.

residence times correspond to mean flow velocities of 1.1 to 0.275 mm s^{-1}. A wide range of membranes were tested: glass, polyethersulphone, cellulose acetate, anion-exchange or cation-exchange materials. In the present work, only results obtained with cation-exchange and cellulose–acetate membranes will be presented. Membranes of the same type were used for both electrode compartments; in this way, there is always an enrichment zone on one side of the separation chamber and a depletion zone on the other. There was no sample injection.

3. MATHEMATICAL MODEL

In the model used, the coupled Navier–Stokes and heat transfer equations are solved numerically by a method closely related to that proposed by Patankar [4]. Details concerning the formulation, the boundary conditions and the numerical techniques employed have already been given [1]. It is sufficient to recall that x is the axis in the direction of carrier flow, y in the direction of the field, and z is in the direction of the chamber thickness. Dimensionless variables were used, among which the velocity vector, in particular, was normed with respect to the mean carrier velocity.

In the present work, a cell geometry somewhat different from that of the previous work was used so as to fit the experimental apparatus. As the electrodes were shorter than the overall chamber length, the only part of the chamber considered in the calculation was that to which the electric field was applied (the 'field zone'). In this chamber, only the back wall is cooled, but this cooling is very efficient as the wall is a metal plate covered by only a thin, electrical insulation layer. This is represented by a correspondingly small thermal resistance. However, the front wall is a thick, uncooled block of plastic material; so this wall was taken as being adiabatic. This arrangement is different from that previously considered, in which the chamber was cooled in the same manner on both walls [1], so in the present calculations no use was made of a plane of symmetry in the centre of the cell.

The electrical resistance of the membranes was calculated from the overall potential difference applied, the potential sums for each row of sensing electrodes and the current densities for each row. Heat generation within the membranes was small enough to be neglected.

The solution density was represented by an empirical function of both temperature and concentration

$$\rho = \rho_w(T) + \beta c. \tag{1}$$

The value of the coefficient β was taken from tabulated values of solution density. From the measured conductivity κ, and the calculated temperature T, the solute concentration c was estimated to satisfy the following expression:

$$\kappa = [\Lambda^0(T) - A(T)\sqrt{c}]c \tag{2}$$

where Λ^0 is the limiting molar conductivity at infinite dilution and A is the Kohlrausch factor (the variation of these variables with temperature being represented by empirical functions). The concentration was assumed not to vary with z. Then the density was calculated from this concentration and the calculated temperature using expression (1). During the iterations of the program, a harmonization of these values according to (1) and (2) was attained.

The grid used had the following number of points: 20, 70 and 16 along the x, y and z axes, respectively. The $x = 0$ plane is at the entrance to the field zone, $x = 250$ mm is the outlet plane for this zone; $z = 0$ is the adiabatic (front) wall and $z = 1$ mm is the cooled (back) wall. In the figures, each line corresponds to one grid line.

In order to ensure a satisfactory convergence of the numerical calculations, it was found that the experimental conductivity data had to be smoothed by taking a local mean. In the smoothed profile, the points at either end of each profile are unmodified; otherwise the number of points used to make the mean was 3, 5 or 7, depending on the number of nearest neighbours available. At the entrance to the field zone, the conductivity was taken as uniform across the chamber width, while at the outlet plane, the profile from the previous row was used. These features can be seen in Figs. 2, 3 and 4. To calculate the conductivity at each grid point, a linear interpolation from the smoothed profiles was applied.

An electro–osmotic slip velocity at the wall in the field direction was assumed to be present due to fixed charges on the chamber wall. The electro–osmotic mobility was taken to be 10^{-8} m^2 V^{-1} s^{-1}. This is the order of magnitude of values previously measured by performing continuous-flow electrophoresis with an uncharged solute [5]. The precise value is difficult to determine, but this is of little importance in the present case as the electro–osmotic flow has little effect on the heat transfer or on the natural convection.

The above calculation gave as output the values of the three components of the liquid velocity and the solution temperature at each grid point.

4. RESULTS

Three figures giving representative experimental results and two series of figures with results of calculations will be shown here. They give a good idea of the interaction between membrane polarization and the flow pattern in this type of CFE equipment. In interpreting these figures, it may be useful to note that at the temperatures considered, a temperature change of 1 K produces a change in density of about 0.1 kg m^{-3}, while the change in solute concentration from its bulk value to 0 corresponds to a density difference of about 0.15 kg m^{-3}.

To demonstrate the effect of a strong concentration polarization, cation-exchange membranes were used. These produce a highly resistant depletion layer with

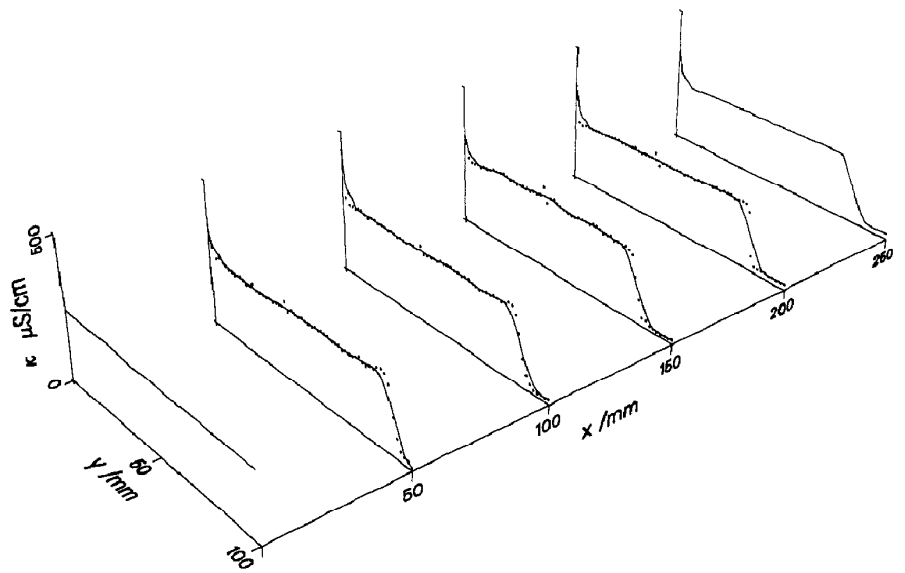

FIG. 2. Experimentally measured conductivities (points) and smoothed values (lines) used as input for the numerical hydrodynamics calculation. Electrolyte: Tris/HNO_3, 5×10^{-3} mol l^{-1}. Cation-exchange membranes. Mean flow velocity: 1.1 mm s^{-1}. Applied potential difference: 368 V. Current density: 30 A m^{-2}. Cooling temperature: 9.6°C.

a concentrated enrichment zone. The experimental conductivity profiles obtained in a typical case with these membranes are shown in Fig. 2. The development of the diffusion layers near the membranes as a function of distance from the beginning of the field zone can be clearly seen: there is a tendency for them to become deeper and wider. An asymmetry between the layers is also visible: the depletion layer is much more pronounced. This is probably due to the fact that as the depletion layer is a low-conductivity region, it is also a zone of high field strength. This means that the ion transfer by migration is much faster there than in the rest of the chamber.

The presence of a certain level of noise in the untreated experimental data can be seen. This prevented the use of the original data in the calculations, as this noise reappeared in the convergence criterion and so masked the presence of incoherences due to incom-

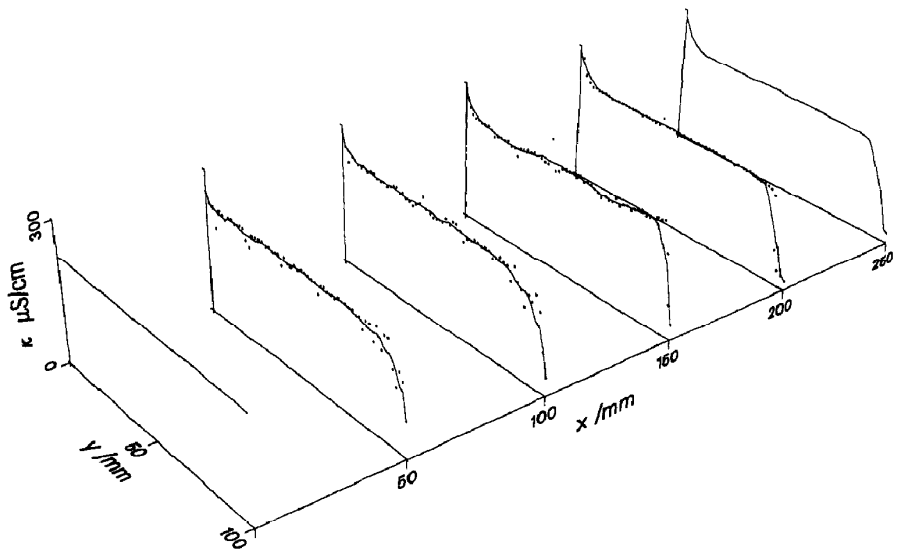

FIG. 3. Experimentally measured conductivities (points) and smoothed values (lines) used as input for the numerical hydrodynamics calculation. Electrolyte: Tris/HAc, 5×10^{-3} mol l^{-1}. Cellulose-acetate membranes. Mean flow velocity: 0.55 mm s^{-1}. Applied potential difference: 180 V. Current density: 30 A m^{-2}. Cooling temperature: 10°C.

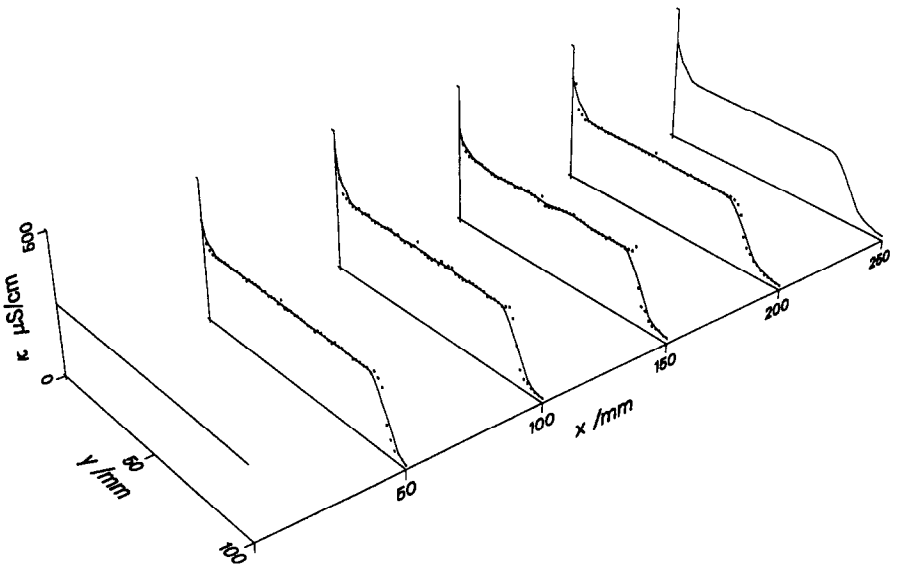

FIG. 4. Experimentally measured conductivities (points) and smoothed values (lines) used as input for the numerical hydrodynamics calculation. Electrolyte: Tris/HAc, 5×10^{-3} mol l^{-1}. Cellulose–acetate membranes. Mean flow velocity: 0.275 mm s^{-1}. Applied potential difference: 270 V. Current density: 30 A m^{-2}. Cooling temperature: 10°C.

plete convergence. Various smoothing techniques were tried, but the best results were obtained by using a local mean, as already mentioned. This process may have led to a slight loss of information but it can be seen that the smoothed curves remain quite faithful to the trend of the measured data.

The temperature distribution over the surface of the uncooled front wall of the chamber is presented in Fig. 5. The quantity plotted is the temperature difference between the carrier solution and the cooling liquid. There is a quite substantial temperature rise in the depletion layer. This is a case in which the density of energy dissipation by Joule heating is particularly high.

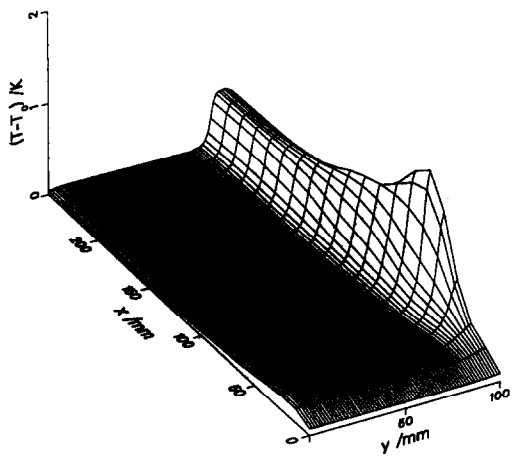

FIG. 5. Temperature T at the inner surface of the front plate (K). T_0 is the temperature of the cooling liquid. Conditions as in Fig. 2.

Figure 6 shows the dimensionless vertical velocity component for the carrier solution in the plane located mid-way between the two walls of the chamber, i.e. the plane where this component has its highest values. The temperature variations seen in the previous figure are found to have very little effect on the carrier flow; its velocity is quite uniform. This is probably because the forced convection velocity (1.1 mm s^{-1}) is relatively high in this case. There is a slight reduction in velocity in the depletion layer and this is clearly seen in Fig. 7, which represents the distribution of the same component over a horizontal cross section near the middle of the chamber. Here it is clear that the temperature gradient between the front ($z = 0$) and back ($z = 1$ mm) walls of the chamber causes no distortion of the parabolic velocity profile in the z direction.

Whereas the results presented so far concern a case where ion-exchange membranes were used, Figs. 3 and 4 show conductivity profiles observed with cellulose–acetate membranes. These membranes have a much lower concentration of fixed charges than the cation-exchange membranes and so cause a lesser degree of concentration polarization. However, a comparison of Fig. 4 with Fig. 2 shows behaviour that is not very different. A quite marked depletion layer is present in Fig. 4, with the same characteristic asymmetry between this layer and the enrichment layer. That the importance of the polarization in Fig. 4 is due to the low flow rate imposed can be seen by a comparison with Fig. 3; at a flow rate twice as high and with the same current density, the observed polarization is much less important, also the asymmetry between the two opposite layers is less pronounced. We shall now see what heat transfer and flow field is

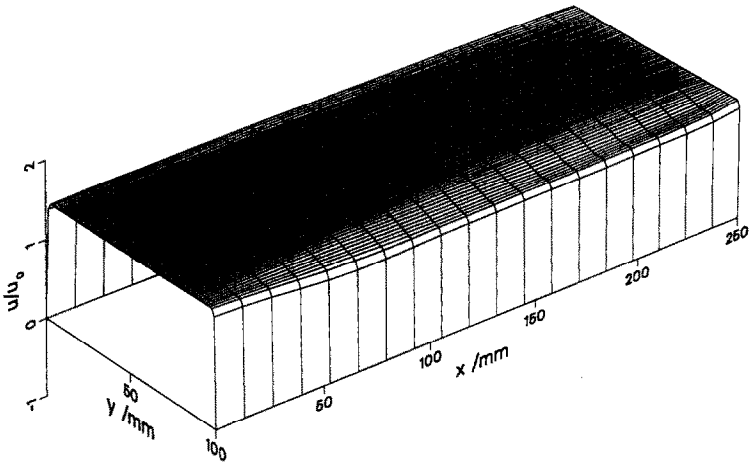

FIG. 6. Dimensionless axial velocity component in the central plane of the chamber (at $z = 0.5$ mm). Conditions as in Fig. 2.

indicated by the numerical model under conditions corresponding to those of Fig. 4.

Figure 8 shows the temperature distribution on the inner face of the uncooled front wall of the chamber; this result should be compared with that shown in Fig. 5. With the cellulose acetate membranes, the lower concentration polarization is reflected in a much smaller variation in temperature (here, a maximum rise of about 0.8 K in the depletion layer). As in the case of the cation-exchange membranes (Fig. 5), the temperature gradient in the flow direction (x-direction) is strongest in the region where the depletion layer is developing, giving rise to a peak at the point where the effect of the natural convection on the axial flow begins to appear. This can be seen from a comparison with Fig. 9.

In Fig. 9, we see the distribution of the axial velocity component over the central plane of the chamber. Here the effect of the buoyancy-driven convection of the axial carrier flow is most apparent. The strongest effect is the reduction of flow velocity in the depletion layer, but a slight acceleration of the flow can be seen in the enrichment layer. The slight velocity fluctuations visible in the central part of the chamber are due to the residues of noise left in the conductivity profiles after smoothing. So here we have a case where the flow field is particularly sensitive to variations in carrier concentration.

The disturbance in the carrier flow is particularly apparent in Fig. 10, illustrating the variation of the axial velocity component over a horizontal cross section, at $x = 200$ mm from the beginning of the field zone.

The disturbed flow field in this case causes a modification in the lateral (y) component of the velocity. Under less disturbed conditions, this component is mainly due to the electro–osmotic flow, but in the present case the parabolic flow profile in the field

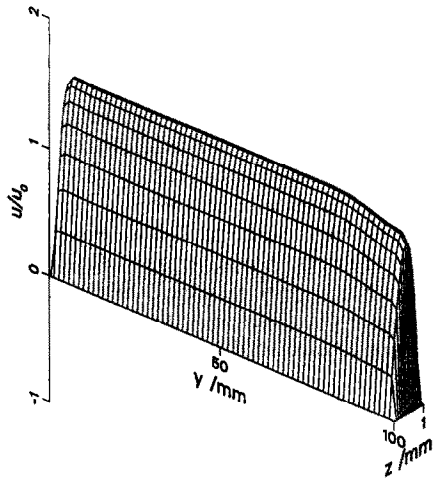

FIG. 7. Dimensionless axial velocity component in a horizontal cross section (at $x = 150$ mm). Conditions as in Fig. 2.

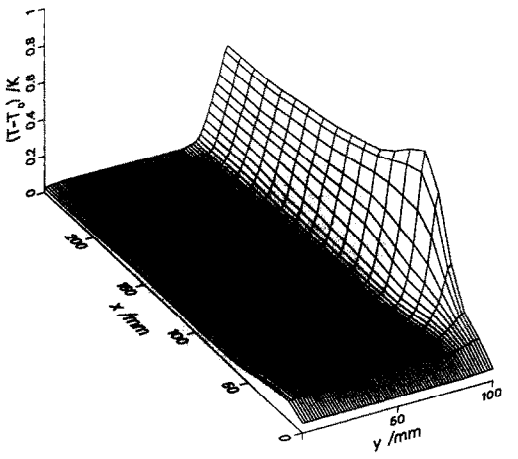

FIG. 8. Temperature T at the inner surface of the front plate (K). T_0 is the temperature of the cooling liquid. Conditions as in Fig. 4.

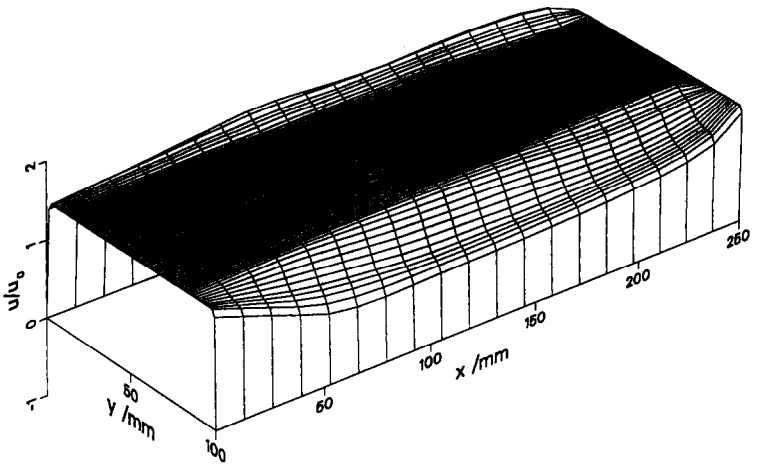

FIG. 9. Dimensionless axial velocity component in the central plane of the chamber (at $z = 0.5$ mm). Conditions as in Fig. 4.

direction is intensified in the upper part of the chamber and attenuated in the lower region. This is the result of the circular convection cell that is superimposed onto the main laminar flow pattern [1].

5. DISCUSSION

On the whole, it can be seen that in the results presented in Figs. 2, 5–7, the flow field is only slightly disturbed, and this even with highly charged membranes known to cause strong concentration polarization. This result is explained by the relatively high forced flow velocity used (1.1 mm s^{-1}), i.e. by the rather short residence time (only 227 s in the field zone). In the second series of results presented here (Figs. 4, 8–10), it was shown that even with much less charged membranes and with a lower rate of heat dissipation, a strongly disturbed flow appears when a low flow rate is imposed so as to obtain a longer residence time. This is an important point as the lengthening of the residence time is one way of improving resolution in this process.

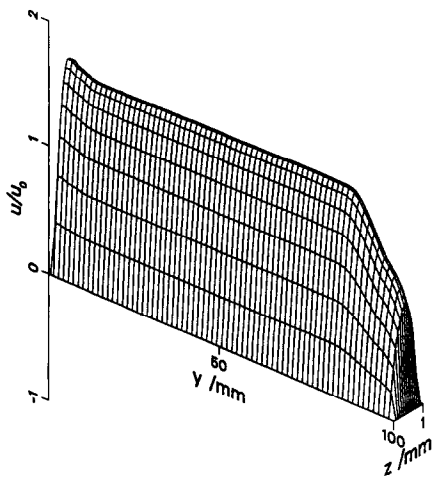

FIG. 10. Dimensionless axial velocity component in a horizontal cross section (at $x = 150$ mm). Conditions as in Fig. 4.

The effect of the longer residence times is not only to make the flow more sensitive to concentration polarization but also to magnify the polarization effect itself. This is clear from Figs. 3 and 4; with residence times in the field zone of 454 and 909 s, respectively. One important element missing from the present work is the lack of coupling in the numerical model between the flow field and the mass transfer in the membrane polarization layers. In fact, since the conductivity profiles used here as a basis for calculation were ones observed experimentally under steady-state conditions, the omission of this coupling is not of great importance within the limits of the present work. Both the experimental observations and the satisfactory convergence of the steady-state calculations indicate that the situations presented here were stable ones. But it is clear from what we have seen, that this coupling between mass transfer and hydrodynamics would be a potential source of instability. To explore all possible operating conditions, a three-dimensional transitory model would then be required, but it would be costly both to write and to exploit. In principle, such a model would make it possible to define precisely under what conditions unsteady flow appears in CFE. But it is already obvious that the conditions shown by Fig. 4 are not far from the unstable state that would prevent any satisfactory separation by CFE.

An important aspect of the present work is that the experimental observations were performed specifically with a commercial chamber designed to provide a good flow stability. The design elements responsible for this are the very efficient cooling system which allows a quite uniform temperature regime to be achieved, even when the rate of energy dissipation is high (i.e. at high field strengths and conductivity), and the relatively small chamber thickness. However from

Figs. 4, 8–10, it is clear that even with good temperature control, the length of residence time available is limited. Furthermore, the use of such a thin chamber, though very effective in stabilizing flow [1, 6], creates other problems with CFE separation as it favours the wall effects known as 'crescent deformation' [6, 7].

The choice of the membranes for the electrode compartments is often seen as an important element in controlling buoyancy-driven convection in CFE. In fact, the membrane properties sought are somewhat contradictory. Generally, the membranes having the required rigidity and mechanical strength (e.g. ion-exchange or glass membranes), also have a high concentration of fixed charge. The less charged membranes (e.g. cellulose or cellulose–acetate) tend to be more fragile. The present work shows that even low-charge membranes are no guarantee against flow instability due to polarization phenomena. But if the results of Figs. 2 and 4 are both considered to be close to the limit of stability (this is less obvious in Fig. 2, but probably true), then for a similar field strength, the less charged membranes allow roughly a four-fold gain in residence time. This, however, is paid for by the inconvenience caused by a less durable membrane material.

The lack of symmetry between enrichment and depletion layers shows that the latter pose greater problems in the way of temperature variation and flow instability. If ion-exchange membranes are used, then it is possible to put a cation-exchange membrane at the anode compartment and an anion-exchange membrane at the cathode; in this way, only enrichment layers are formed in the separation chamber. This is particularly advantageous in the down-flow mode of operation used here. But there can still be sufficient natural convection to introduce uncertainties as to the effective residence time experienced by the protein [8]. Furthermore, no exact symmetry in behaviour between the two membranes can be expected.

6. CONCLUSION

The experimental results presented here have shown how, in CFE, the ion transfer between the separation chamber and the electrode compartments can create important changes in carrier conductivity. This concentration polarization at the membranes not only introduces non-uniformities in the field strength, but as the numerical calculations have shown, can also give rise to temperature gradients and flow disturbances that are very harmful to the correct functioning of the CFE process. It was also seen experimentally that the flow field strongly effects the degree of polarization: so the feedback loop of concentration polarization giving a disturbed flow field which itself tends further to enhance polarization, can be an important source of flow instability even in a CFE chamber designed to minimize it. The operating conditions used in this work are close to those generally applied with this sort of equipment, so the presence of this instability creates a real limitation to the application of the CFE process. The use of less charged membranes provides only a partial answer to this problem. Of course, the use of CFE under microgravity conditions would eliminate the problems raised by buoyancy forces and the possibility is being seriously investigated, but the cost of this solution remains extremely high.

Acknowledgement—For one of us (M. J. C.), this work was financed by a contract with the Centre National d'Etudes Spatiales (CNES), the French space agency.

REFERENCES

1. N. Jouve and M. J. Clifton, Three-dimensional modelling of the coupled flow field and heat transfer in continuous-flow electrophoresis, *Int. J. Heat Mass Transfer* **34,** 2461–2474 (1991).
2. J. Heinrich and H. Wagner, Deutsches Patent 3931851 (1989).
3. J. Heinrich and H. Wagner, A potential-gradient conductivity scanner for the investigation of effects leading to buoyancy-driven convection in continuous-flow electrophoresis, *Adv. Space Res.* **12,** 385–392 (1992).
4. S. V. Patankar, *Numerical Heat Transfer and Fluid Flow*. Hemisphere, New York (1980).
5. M. J. Clifton, N. Jouve, H. de Balmann and V. Sanchez, Conditions for purification of proteins by free-flow zone electrophoresis, *Electrophoresis* **11,** 913–919 (1990).
6. D. A. Saville, The fluid mechanics of continuous flow electrophoresis in perspective, *Physicochem. Hydrodyn.* **1,** 297–307 (1980).
7. A. Strickler and T. Sacks, Focusing in continuous-flow electrophoresis systems by electrical control of effective cell wall zeta potentials, *Ann. N.Y. Acad. Sci.* **209,** 497–514 (1973).
8. M. J. Clifton, N. Jouve and V. Sanchez, Influence of buoyancy-driven convection on protein separation by free-flow electrophoresis, *Adv. Space Res.* **12,** 373–383 (1992).